



1 The general formulation for runoff components estimation

2 and attribution at mean annual time scale

Yufen He¹, Changming Li^{1*}, Hanbo Yang^{1*}

4 1 State Key Laboratory of Hydroscience and Engineering, Department of Hydraulic Engineering,
5 Tsinghua University, Beijing 100084, China

6 *Correspondence: Changming Li (licm_13@163.com), Hanbo Yang
7 (yanghanbo@tsinghua.edu.cn)

8 Abstract

9 Estimating runoff components, including surface flow, baseflow and total runoff is essential for
10 understanding precipitation partition and runoff generation and facilitating water resource
11 management. However, a general framework to quantify and attribute runoff components is still
12 lacking. Here, we propose a general formulation through observational data analysis and
13 theoretical derivation based on the two-stage Ponce-Shetty model (named as the MPS model).
14 The MPS model characterizes mean annual runoff components as a function of available water
15 with one parameter. The model is applied over 662 catchments across China and the contiguous
16 United States. Results demonstrate that the model well depicts the spatial variability of runoff
17 components with R^2 exceeding 0.81, 0.44 and 0.80 for fitting surface flow, baseflow and total
18 runoff, respectively. The model effectively simulates multi-year runoff components with R^2
19 exceeding 0.97, and the proportion of runoff components relative to precipitation with R^2
20 exceeding 0.94. By using this conceptual model, we elucidate the responses of surface flow and
21 baseflow to available water and environmental factors for the first time. The surface flow is
22 jointly controlled by precipitation and environmental factors, while baseflow is mainly influenced
23 by environmental factors in most catchments. The universal and concise MPS model offers a new
24 perspective on the long-term catchment water balance, facilitating broader application in
25 large-sample investigations without complex parameterizations and providing an efficient tool to
26 explore future runoff variations and responses under changing climate.



27 **Key Points**

28 (1) A general and concise formulation is proposed to quantify, and attribute mean annual
29 surface flow, baseflow and total runoff.

30 (2) The formulation characterizes runoff components as a function of available water without
31 additional and complicated parameter calculation.

32 (3) The formulation performs well in quantifying and attributing runoff components in 662
33 catchments.

34 **1. Introduction**

35 Runoff is the primary freshwater resource accessible for human life and plays an essential role
36 in the water cycle (He et al., 2022; Wang et al., 2024). Based on the propagation time and
37 hydraulic response of a catchment, total runoff (Q) can be divided into baseflow (Q_b) and surface
38 flow (Q_s) (Gnann et al., 2019; Singh et al., 2019). Baseflow, also referred to as slow flow, is
39 defined as the flow that originates from groundwater and other delayed sources (such as wetlands,
40 lakes, snow and ice), and generally sustains streamflow during dry periods (Gnann, 2021; Hall,
41 1968). Baseflow is the relatively stable component of runoff, playing a vital role in aquatic
42 ecosystems (de Graaf et al., 2019; Price et al., 2011), water quality (Ficklin et al., 2016) and
43 sustained water supplies (Fan et al., 2013). Surface flow, also referred to as fast flow, results from
44 rapid processes like the saturation or infiltration of excess overland flow and swift subsurface
45 flow (Beven and Kirkby, 1979), leading to immediate water movement. Surface flow occurs more
46 rapidly and with more drastic changes than baseflow, which is primarily responsible for flood
47 generation (Yin et al., 2018) and soil erosion (Morgan, 2011).

48 Most current studies focus on total runoff variability and attribution, and the relevant
49 researches are fairly mature (Berghuijs et al., 2017; Han et al., 2023; Liu et al., 2021). However,
50 few studies pay attention to comprehensive research on the different runoff components (Li et al.,
51 2020; Liu et al., 2019), and the attributions of Q_s and Q_b changes are still unclear (Hellwig and
52 Stahl, 2018). Baseflow and surface flow represent different hydrological processes, and their
53 implications for watershed management are also not identical (Zheng Mingguo, 2014). For



example, the research conducted by Ficklin et al. (2016) in the United States points out apparent spatial differences between Q_b and Q_s in different seasons. Therefore, it is necessary to quantify runoff components and distinguish their controlling factors to better understand the runoff dynamics and facilitate water resources management in the context of intensified climate change and anthropogenic disturbance.

Unlike Q , which is ascertainable through direct observation at hydrological gauges, Q_b and Q_s can only be estimated through indirect methods, including baseflow separation (Wu et al., 2019; Zhang et al., 2017), isotope tracing (Hale et al., 2022; Wallace et al., 2021) and hydrological modeling (Al-Ghobari et al., 2020; Cheng et al., 2020; Huang et al., 2007; Kaleris and Langousis, 2017). The first two methods estimate Q_b initially, and Q_s is then derived as the difference between the Q and the estimated Q_b , limiting their ability to examine the dynamic variations of each runoff component independently, and the isotope tracing method is challenging to conduct on a large and long-term scale. The hydrological modeling enables to simulate Q_b and Q_s separately, typically reflected in different modules and empirical formulations. In hydrological models, Q_b is encoded using linear or non-linear storage-discharge functions (Chen and Ruan, 2023; Cheng et al., 2020). Q_s is closely related to rainfall, but the models for estimating it are usually event-based (such as the Soil Conservation Service Curve Number method (Al-Ghobari et al., 2020; SCS, 1972; Shi et al., 2017) and very few studies explored the controls on the mean annual Q_s (Neto et al., 2020). Among various models, the Budyko framework (Budyko, 1974) in conjunction with water-energy balance method (Choudhury, 1999; Yang et al., 2008) (see the second row in Table 1), has been widely used in the analysis of mean annual Q due to its simple, universal and transparent characteristics (He et al., 2022; Roderick and Farquhar, 2011).

Recently, utilizing the extended Budyko framework to estimate Q_b and Q_s has attracted attention. Wang and Wu (2013) and Neto et al. (2020) established the regression relationship between baseflow fraction (BFC , the ratio of Q_b to precipitation (P)) and aridity index (ϕ , the ratio of mean annual potential evapotranspiration (E_0) to P) using analytical formulation. However, Gnann et al. (2019) reported that using only the ϕ struggles to delineate baseflow variability in humid catchments, where the impact of soil water storage capacity (S_p) is as critical as that of the ϕ . Thus, Cheng et al. (2021) proposed an analytical curve for describing mean annual Q_b by introducing S_p as another theoretical boundary. Results show that the developed



84 curve agrees well with the observed BFC ($R^2 = 0.75$, $RMSE = 0.058$) and Q_b ($R^2 = 0.86$,
85 $RMSE = 0.19$ mm), outperforming the original Budyko framework. Analogously, Yao et al.
86 (2021) derived similar functions incorporated the ϕ , S_p and a shape parameter to model BFC and
87 baseflow index (BFI , the ratio of Q_b to Q). These extended Budyko frameworks accounting for S_p
88 have advantages in simulating Q_b . However, S_p is challenging to obtain through observations and
89 often requires calibration (Cheng et al., 2021) or computation (Yao et al., 2021), adding certain
90 uncertainties to the model. Notably, the calibration performance of Q_s in equation (1) to obtain W_p
91 (the proxy of S_p) in the catchments of China are not always satisfactory, especially in the northern
92 catchments (Figure S1). Moreover, the complicated forms can bring inherent uncertainties and
93 these studies have not validated the formulations of Q_s , which are derived by subtracting Q_b from
94 Q or fitting curves (Cheng et al., 2021; Neto et al., 2020), implying that they may overlook the
95 physical processes represented by surface flow. In the subsequent discussion, the Budyko
96 framework and extended Budyko equations are collectively referred to as the "Budyko-type
97 formulations" (Table 1).

98 Many researchers have observed similar behavior of Q_b to Q (Cheng et al., 2021; Gnann et al.,
99 2019; Wang and Wu, 2013). Is there a similar behavior for Q_s ? In a two-stage partitioning theory
100 (L'vovich, 1979), runoff components are delineated based on the available water at each stage.
101 Therefore, is there a general framework to unify different runoff components? Although various
102 functional forms have been proposed for estimating runoff components in the literature, a
103 universal method that reveals the mechanisms of mean annual runoff components generation and
104 subsequent quantification and attribution is still in need.

105 **Table 1.** The Budyko-type formulations for estimating mean annual runoff components

References	Formulations	Parameters
Choudhury (1999); Yang et al. (2008)	$Q = P - \frac{P \times E_0}{(P^n + E_0^n)^{1/n}}$	n
Wang and Wu (2013)	$\frac{Q_b}{P} = 1 - \left[1 + \left(\frac{E_0}{P} \right)^{-v} \right]^{-1/v}$	v
Neto et al. (2020)	$f_s(\phi) = \exp(-\phi^a + \delta_s)^b$ $f_b(\phi) = \exp(-\phi^c + \delta_b)^d$	a, b, c, d $\delta_s = \ln \left(\left[\frac{\bar{Q}_s}{P} \right]_{max} \right)^{1/b}$



$$\delta_B = \ln \left(1 - \left[\frac{\bar{Q}_S}{P} \right]_{max} \right)^{1/d}$$

$$\frac{Q_s}{P} = -\frac{E_0 + S_p}{P} + \left[1 + \left(\frac{E_0 + S_p}{P} \right)^{\alpha_1} \right]^{1/\alpha_1}$$

$$\text{Cheng et al. (2021)} \quad \frac{Q_b}{P} = \frac{S_p}{P} + \left[1 + \left(\frac{E_0}{P} \right)^{\alpha_2} \right]^{1/\alpha_2} - \left[1 + \left(\frac{E_0 + S_p}{P} \right)^{\alpha_2} \right]^{1/\alpha_2}$$

$$Q_b = \frac{P + S_b - \sqrt{(P + S_b)^2 - 2aS_bP}}{a} \quad \left. \begin{array}{l} 1 \\ \\ \frac{1 + \frac{E_0}{P} \frac{P}{S_b} - \sqrt{\left(1 + \frac{E_0}{P} \frac{P}{S_b}\right)^2 - 2a \frac{E_0}{P} \frac{P}{S_b}}}{a} \\ \\ \frac{\frac{P}{S_b} + 1 - \sqrt{\left(\frac{P}{S_b} + 1\right)^2 - 2a \frac{P}{S_b}}}{a} \\ \\ * \frac{E_0 + S_b - \sqrt{(E_0 + S_b)^2 - 2aE_0S_b}}{a} \end{array} \right] \quad S_b, a$$

106 Note that P is the mean annual precipitation, E_0 is the mean annual potential evapotranspiration, $f_S(\phi)$ and
 107 $f_B(\phi)$ are the surface flow and baseflow function, respectively and S_p is the catchment storage capacity.

108 To address these questions, we derived a modified two-stage partitioning framework through
 109 observational data analysis and theoretical derivation based on the Ponce-Shetty model (Ponce
 110 and Shetty, 1995; Sivapalan et al., 2011) (namely the MPS model) at mean annual time scale. The
 111 Ponce-Shetty model is a conceptual model with physical constraint developed at annual scale to
 112 depict how precipitation is partitioned, stored and released in the catchment (Gnann et al., 2019).
 113 It posits that annual precipitation is partitioned into Q_s and soil wetting (W) and, subsequently, the
 114 resulting W is partitioned into Q_b and vaporization (V) (Sivapalan et al., 2011). The MPS model



115 enables large-sample catchments research, which may lead to new understanding of mean annual
116 water balance and allocation.

117 In general, the objectives of this study are to (1) develop a general and concise formulation to
118 describe runoff components variability at mean annual time scale; (2) validate and compare the
119 performance of the developed formulation against Budyko-type formulations; (3) attribute the
120 variations of runoff components induced by the changes of precipitation and other factors. Here,
121 we modify the Ponce-Shetty model according to some conditions and hypothesize a general
122 runoff components model (the MPS model), that describes Q_s , Q_b and Q as a function of
123 respective available water with one parameter. The MPS model is then validated over 662
124 catchments across China and the contiguous United States (the CONUS) over a wide range of
125 hydro-meteorological circumstances. The performance of the MPS model is also compared with
126 the Budyko-type formulations. Section 2 introduces the derivation of the MPS model. Section 3
127 provides the study catchments, data and the parameter estimation technique. Section 4 shows the
128 results followed by a discussion in Section 5. The conclusions are summarized in Section 6.

129 **2. Derivation of the Modified Ponce-Shetty Model**

130 L'vovich (1979) proposed a conceptual theory for the two-stage catchment water balance
131 partition at the annual time scale according to Horton's approach (Horton, 1933). Firstly,
132 precipitation is partitioned into surface flow (Q_s) and catchment wetting (W , stored water), and
133 then, the catchment wetting is partitioned into baseflow (Q_b) and vaporization (V , including
134 interception loss, evaporation and transpiration). Ponce and Shetty (1995) conceptualized the
135 partition of each step as the form of a competition, and derived the formulations of runoff
136 components based on the proportionality hypothesis. Sivapalan et al. (2011) reintroduced the
137 Ponce-Shetty equations as follows:

138 In the first stage, $P = Q_s + W$:

$$Q_s = \begin{cases} 0, & \text{if } P \leq \lambda_s W_p \\ \frac{(P - \lambda_s W_p)^2}{P + (1 - 2\lambda_s)W_p}, & \text{if } P > \lambda_s W_p \end{cases} \quad (1)$$



$$W = \begin{cases} P, & \text{if } P \leq \lambda_s W_p \\ P - \frac{(P - \lambda_s W_p)^2}{P + (1 - 2\lambda_s)W_p}, & \text{if } P > \lambda_s W_p \end{cases} \quad (2)$$

$$P \rightarrow \infty, Q_s \rightarrow P - W_p, W \rightarrow W_p \quad (3)$$

139 In the second stage, $W = Q_b + V$:

$$Q_b = \begin{cases} 0, & \text{if } W \leq \lambda_b V_p \\ \frac{(W - \lambda_b V_p)^2}{W + (1 - 2\lambda_b)V_p}, & \text{if } W > \lambda_b V_p \end{cases} \quad (4)$$

$$V = \begin{cases} W, & \text{if } W \leq \lambda_b V_p \\ W - \frac{(W - \lambda_b V_p)^2}{W + (1 - 2\lambda_b)V_p}, & \text{if } W > \lambda_b V_p \end{cases} \quad (5)$$

$$W \rightarrow \infty, Q_b \rightarrow W - V_p, V \rightarrow V_p \quad (6)$$

140 where λ_s and λ_b are the surface flow and baseflow initial abstraction coefficients, respectively,
 141 which range from 0 to 1. The larger value of λ , the more difficult it is to generate flow. W_p and V_p
 142 are catchment wetting potential and vaporization potential, respectively, which are greater than 0.
 143 The relative $\lambda_s W_p$ and $\lambda_b V_p$ are the surface flow and baseflow generation thresholds,
 144 respectively.

145 Note that the interannual water storage change is supposed to be negligible (Ponce and Shetty,
 146 1995). In a companion paper of Sivapalan et al. (2011), Harman et al. (2011) employed the
 147 annual Ponce-Shetty model at mean annual time scale and validated its applicability. Using the
 148 first phase as an example, Q_s can be considered a function of λ_s , denoted as $f(\lambda_s)$:

$$f(\lambda_s) = \begin{cases} 0, & \text{if } \lambda_s \geq P/W_p \\ \frac{(P - \lambda_s W_p)^2}{P + (1 - 2\lambda_s)W_p}, & \text{if } \lambda_s < P/W_p \end{cases} \quad (7)$$

149 When $\lambda_s < P/W_p$, the Taylor expansion of $f(\lambda_s)$ at $\lambda_s=0$ is:

$$f(\lambda_s) = f(0) + f'(0) * \lambda_s + \frac{f''(0)}{2!} * \lambda_s^2 + \dots + \frac{f^n(0)}{n!} * \lambda_s^n + \dots \quad (8)$$

150 Hence, we have the zeroth-order approximation:

$$f(\lambda_s) \approx \frac{P^2}{P + W_p} \quad (9)$$



151 When the remainder term is relatively small, an approximation equation can be used to
152 estimate the multi-year Q_s as:

$$Q_s = \frac{P^2}{P + W_p} \quad (10)$$

153 In addition, the zeroth-order approximation of Q_b can be similarly obtained as:

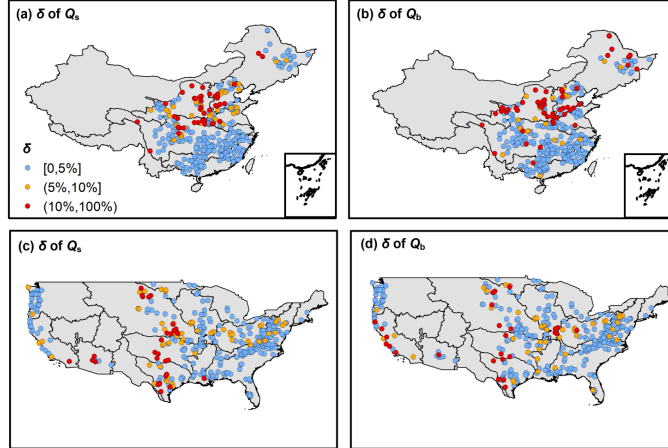
$$Q_b = \frac{W^2}{W + V_p} \quad (11)$$

154 To evaluate the impact of the remainder term, we calculate the relative bias (δ) of runoff
155 components for 312 basins in China and 350 basins in the United States using the approximate
156 equations (Eq (10) and Eq (11)) and the original Ponce-Shetty equations (Eq (1) and Eq (4)) (data
157 sources in Section 3.1). The parameters in the original Ponce-Shetty equations are calibrated
158 using the nonlinear least squares method. The δ is calculated as:

$$\delta = \frac{|\widetilde{Q}_y - Q_y|}{Q_y} \quad (12)$$

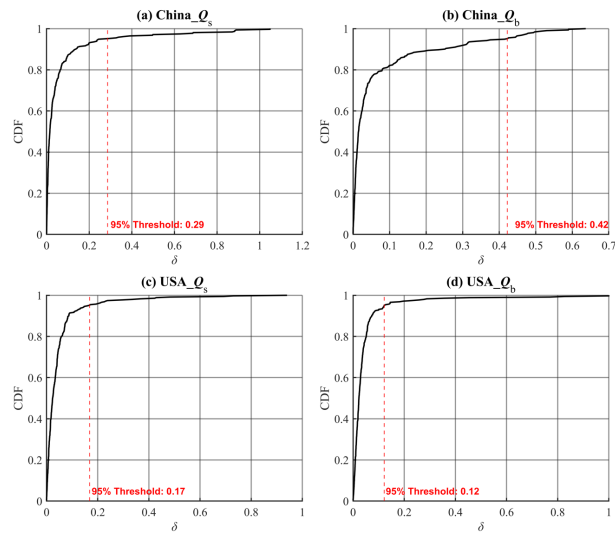
159 where Q_y represents runoff components estimated by the Ponce-Shetty equations, and \widetilde{Q}_y
160 represents runoff components estimated by the approximate equations (Eq (10) and Eq (11)).

161 The spatial distribution of δ and the cumulative distribution functions (CDFs) of δ are
162 shown in Figure 1 and Figure 2, respectively. As shown in Figure 1, 77% of the basins have an δ
163 of less than 5%. The average δ for estimating Q_s is 6.5% in China and 4.8% in the United States,
164 while the average δ for estimating Q_b is 7.9% in China and 6.6% in the United States, with
165 larger deviations observed in arid basins. Figure 2 indicate that the δ values for the approximate
166 model are within acceptable limits across both China and CONUS. The relatively low 95%
167 threshold values, particularly for the USA datasets, suggest that the majority of predictions fall
168 within a narrow error range, indicating robust model performance. This acceptability of δ across
169 regions and variables highlights the approximate equations' capability to maintain prediction
170 accuracy under varying geographical and hydrological conditions, indicating that the Zeroth-order
171 approximation is representative for the original Ponce-Shetty model.



172

173 **Figure 1.** The distribution of relative bias (δ) between the results by the approximate equations
174 (Eq (10) and Eq (11)) versus the original Ponce-Shetty equations (Eq (1) and Eq (4)). The first
175 row shows the results for 312 basins in China, and the second row shows the results for 350
176 basins in CONUS. The first column corresponds to surface flow (Q_s), and the second column
177 corresponds to baseflow (Q_b).



178

179 **Figure 2.** Cumulative distribution functions (CDFs) of the relative bias (δ) for each dataset,
180 represented by four subplots corresponding to different regions and variables: (a) China_ Q_s , (b)
181 China_ Q_b , (c) USA_ Q_s , and (d) USA_ Q_b . Each subplot includes a red dashed line indicating the
182 95% δ threshold



183 Therefore, we can approximately consider that on a multi-year scale, Q_s and Q_b can be
184 estimated using the zeroth-order approximation in Eq (10) and Eq (11). We subsequently assume
185 a similar formulation of mean annual Q :

$$Q = \frac{P^2}{P + U_p} \quad (13)$$

186 where U_p is the parameter representing the upper limit of the portion remaining after precipitation
187 is allocated to runoff, hereafter we refer to U_p as evapotranspiration potential.

188 Integrating equations (10), (11) and (13), we conclude a general formulation to depict
189 multi-year variability of runoff components and their quantification, hereafter referred to as the
190 modified Ponce-Shetty model (the MPS model):

$$Q_y = \frac{X^2}{X + M} \quad (14)$$

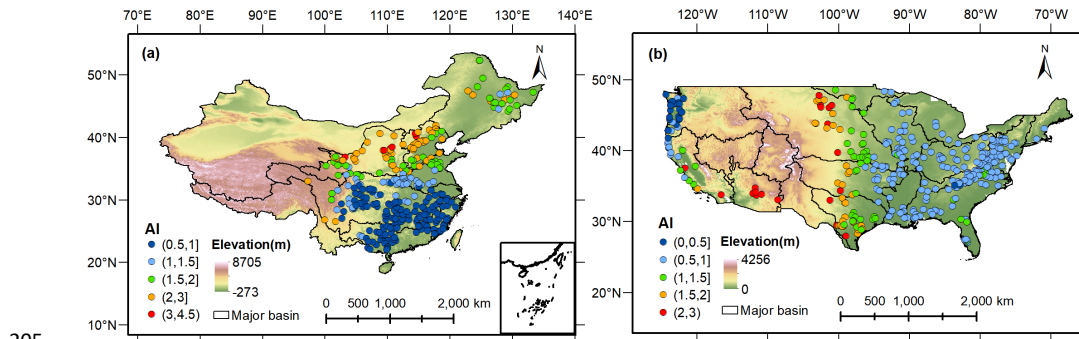
191 where Q_y represents runoff components (i.e., Q , Q_s , Q_b), X corresponds to the available water of
192 each runoff component, i.e., P is the available water of Q and Q_s , and W the available water of Q_b .
193 M is an integrated parameter, representing the comprehensive effects of catchment characteristics
194 and atmospheric water and energy demand.

195 The MPS model encodes runoff components as a function of available water with only one
196 parameter, which not only considers processes of runoff generation with physical constraints, but
197 also, compared to the Budyko-type formulations and the original Ponce-Shetty model, is more
198 concise in form and requires fewer parameters. Therefore, it is possible to estimate the long-term
199 runoff components when only long-term variables are known.

200 3. Data and Methodology

201 3.1. Data

202 To validate the reliability of the MPS model, daily hydrological and meteorological data from
203 312 catchments in China (Li et al., 2024) and 350 catchments in the CONUS are collected. The
204 location of all the catchments hydrological stations is shown in Figure 3.



205
206 **Figure 3.** Location of hydrological stations for the (a) 312 catchments in China and (b) 350
207 catchments in the CONUS, colored by the value of aridity index (ϕ , namely E_0/P).

208 In China, precipitation data at 0.25° spatial resolution are obtained from the China
209 Gauge-based Daily Precipitation Analysis (CGDPA) (Shen and Xiong, 2016). Other
210 meteorological data, including wind speed, sunshine hours, relative humidity, and air temperature,
211 are from about 736 stations of the China Meteorological Data Service Center
212 (<http://data.cma.cn/en>, last access: 11 November 2023). The in-site meteorological data are
213 interpolated into a 10-km grid using the inverse-distance weighted method (Yang et al., 2014).
214 We use the Penman equation (Penman, 1948) to estimate E_0 of each grid. The aridity index ϕ is
215 subsequently calculated as E_0/P . All grid data are aggregated and lumped for individual
216 catchments. The discharge data are collected from the Hydrological Bureau of the Ministry of
217 Water Resources of China (<https://www.mwr.gov.cn/english/>, last access: 20 December 2023)
218 and are selected based on the length of records exceeding 35 years with less than 5% missing data.
219 The time range for all data is 1960-2000.

220 In the CONUS, we use data set from CAMELS (Addor et al., 2017; Newman et al., 2015). The
221 CAMELS data set provides 662 catchments with daily time series of precipitation and observed
222 runoff along with aridity index, and most catchments contain 35 years of continuous runoff from
223 1980 to 2014. The criteria for excluding catchments are referred to Gnann et al. (2019), and
224 finally 350 catchments remained.

225 We use the one-parameter Lyne-Hollick digital filter (Lyne, 1979) to separate daily Q_s and Q_b
226 from daily Q . The Lyne-Hollick method is applied forward, backward, and forward again with a
227 filter parameter of 0.925 and has manifested to be reliable to obtain runoff components (Lee and



228 Ajami, 2023). We use the separated Q_s and Q_b as the reference. Although there are other baseflow
229 separation algorithms, according to Troch et al. (2009), the choice of baseflow separation
230 algorithm is not a significant determinant of the water balance at the annual scale.

231 All the hydrological and meteorological data are aggregated to the annual and mean annual
232 time scales for further analysis.

233 **3.2. Calibration and Validation**

234 Spatially, to verify the MPS model's ability to characterize the variability of runoff components
235 between catchments, we utilize the least squares fitting algorithm to estimate parameters, i.e., W_p ,
236 V_p and U_p . The three parameters are restricted to being between 0 mm and 50, 000 mm, which is
237 considered high enough to not affect the parameter estimation (Gnann et al., 2019).

238 In terms of time, we split all data into two periods for parameter calibration and validation of
239 Eq. (14) for individual catchments. In China, the data ranges from 1960 to 2000, so we use the
240 first 31 years (1960-1990) as the calibration period and the remaining 5-10 years (1991-2000) as
241 the validation period. In the CONUS, the calibration period is chosen as 1980-2000, and the
242 validation period is from 2001 to 2014. When we know mean annual Q_s , Q_b , Q , P and W of the
243 first period, the parameters, i.e., W_p , V_p and U_p , can be derived from Eq. (14). Postulating the
244 parameters remain unchanged during two periods, we consequently can estimate the mean annual
245 Q_s , Q_b and Q of the second period using Eq. (14). Note that the catchment wetting W is calculated
246 as the difference of the P and estimated Q_s .

247 The surface flow fraction (*SFC*, the ratio of surface flow to precipitation) and baseflow fraction
248 (*BFC*, the ratio between baseflow and precipitation) represent the proportion of rainfall becoming
249 different runoff components, which are commonly used to quantify surface flow and baseflow
250 (Wang and Wu, 2013). Therefore, we evaluate the simulation of *SFC* and *BFC* as well as the
251 volume of runoff components.

252 The performance of the MPS model is evaluated by the coefficient of determination (R^2) and
253 the root mean square error (RMSE):

$$R^2 = \left(\frac{\sum_{i=1}^N (X_{sim,i} - \bar{X}_{sim})(X_{obs,i} - \bar{X}_{obs})}{\sqrt{\sum_{i=1}^N (X_{sim,i} - \bar{X}_{sim})^2 \sum_{i=1}^N (X_{obs,i} - \bar{X}_{obs})^2}} \right)^2 \quad (15)$$



$$\text{RMSE} = \sqrt{\frac{1}{N} \sum_{i=1}^N (X_{sim,i} - X_{obs,i})^2} \quad (16)$$

254 where X represents the evaluated variable, i.e., mean annual Q , Q_s and Q_b , SFC and BFC in this
 255 study. The subscript obs and sim represents the observed and simulated value, respectively.
 256 Higher R^2 and lower RMSE indicate good model performance.

257 **3.3. Attribution analysis**

258 We split the data into the first period (1960-1990 in China and 1980-2000 in the CONUS) and
 259 the second period (1991-2000 in China and 2001-2014 in the CONUS) to attribute runoff
 260 components variation between two periods. Note that the attribution of ΔQ is only conducted in
 261 China because the E_0 in CAMELS dataset is a constant in each catchment. In the MPS model, we
 262 consider that the runoff changes between two long-term periods are caused by available water and
 263 other environmental and anthropogenic factors (such as land cover/use change and
 264 evapotranspiration variation) encoded by parameters. For the changes of surface flow (ΔQ_s) and
 265 total runoff (ΔQ), postulating that each variable is independent in the MPS model, the first-order
 266 approximation of the ΔQ_s and ΔQ from the second period to the first period can be expressed as
 267 (Milly and Dunne, 2002):

$$\Delta Q_s = \frac{\partial Q_s}{\partial P} \Delta P + \frac{\partial Q_s}{\partial W_p} \Delta W_p \quad (17a)$$

$$\Delta Q = \frac{\partial Q}{\partial P} \Delta P + \frac{\partial Q}{\partial U_p} \Delta U_p \quad (17b)$$

268 where the two terms on the right side of equation (17a) respectively represent changes in Q_s
 269 caused by changes in P (ΔQ_{s-P}) and other factors (ΔQ_{s-W_p}), and the two terms on the right side
 270 of equation (17b) respectively represent changes in Q caused by changes in P (ΔQ_P) and other
 271 factors (ΔQ_{W_p}). For convenience, we refer partial derivative coefficient $\frac{\partial Q_s}{\partial P}$, $\frac{\partial Q_s}{\partial W_p}$, $\frac{\partial Q}{\partial P}$ and $\frac{\partial Q}{\partial U_p}$ in
 272 equation (17) as ζ_{Qs-P} , ζ_{Qs-W_p} , ζ_{Q-P} and ζ_{Q-W_p} , which can be calculated as:

$$\zeta_{Qs-P} = \frac{P^2 + 2PW_p}{(P + W_p)^2} \quad (18a)$$



$$\zeta_{Qs-Wp} = \frac{-P^2}{(P + W_p)^2} \quad (18b)$$

$$\zeta_{Q-P} = \frac{P^2 + 2PU_p}{(P + U_p)^2} \quad (18c)$$

$$\zeta_{Q-Wp} = \frac{-P^2}{(P + U_p)^2} \quad (18d)$$

273 The changes of baseflow (ΔQ_b) is induced by the variations of the W and V_p . However, we
 274 focus more on the impact of P in application. Therefore, we combine equation (10), (11) and $W =$
 275 $P - Q_s$, so the Q_b can be calculated as :

$$Q_b = \frac{P^2 W_p^2}{(P + W_p)(P W_p + P V_p + W_p V_p)} \quad (19)$$

276 The ΔQ_b can be attributed as the variations of P , W_p and V_p :

$$\Delta Q_b = \frac{\partial Q_b}{\partial P} \Delta P + \frac{\partial Q_b}{\partial W_p} \Delta W_p + \frac{\partial Q_b}{\partial V_p} \Delta V_p \quad (20)$$

277 where the three terms on the right side of equation (20) respectively represent changes in Q_b
 278 caused by changes in P (ΔQ_{b-P}), W_p (ΔQ_{b-Wp}) and V_p (ΔQ_{b-Vp}). The partial derivative
 279 coefficient $\frac{\partial Q_b}{\partial P}$ (ζ_{Qb-P}), $\frac{\partial Q_b}{\partial W_p}$ (ζ_{Qb-Wp}) and $\frac{\partial Q_b}{\partial V_p}$ (ζ_{Qb-Vp}) can be calculated as:

$$\zeta_{Qb-P} = \frac{2P^2 W_p^3 V_p + P^2 W_p^4 + 2P W_p^4 V_p}{(P + W_p)^2 (P W_p + P V_p + W_p V_p)^2} \quad (21a)$$

$$\zeta_{Qb-Wp} = \frac{P^4 W_p^2 + 2P^4 W_p V_p + 2P^3 W_p^2 V_p}{(P + W_p)^2 (P W_p + P V_p + W_p V_p)^2} \quad (21b)$$

$$\zeta_{Qb-Vp} = \frac{-P^2 W_p^2}{(P + W_p)^2 (P W_p + P V_p + W_p V_p)^2} \quad (21c)$$

280 To verify the applicability of the MPS model for runoff components attribution, we compare
 281 the calculated ΔQ_s , ΔQ_b and ΔQ using equation (17) and (20) with the observed ΔQ_s , ΔQ_b
 282 and ΔQ between two periods. The evaluation metrics are R^2 and RMSE.

283 The relative contribution ratios of P and other factors to runoff components change are
 284 calculated as:



$$\eta_P = \frac{\Delta Q_{y-P}}{|\Delta Q_{y-P}| + |\Delta Q_{y-Wp}| + |\Delta Q_{y-Vp}|} \times 100\% \quad (22a)$$

$$\eta_{Wp} = \frac{\Delta Q_{y-Wp}}{|\Delta Q_{y-P}| + |\Delta Q_{y-Wp}| + |\Delta Q_{y-Vp}|} \times 100\% \quad (22b)$$

$$\eta_{Vp} = \frac{\Delta Q_{y-Vp}}{|\Delta Q_{y-P}| + |\Delta Q_{y-Wp}| + |\Delta Q_{y-Vp}|} \times 100\% \quad (22c)$$

285 where η_P , η_{Wp} and η_{Vp} are the relative contribution ratios of P , W_p and V_p to runoff
286 components, respectively. We subsequently use the absolute values of η to identify the dominant
287 factor impacting runoff components.

288 4. Results

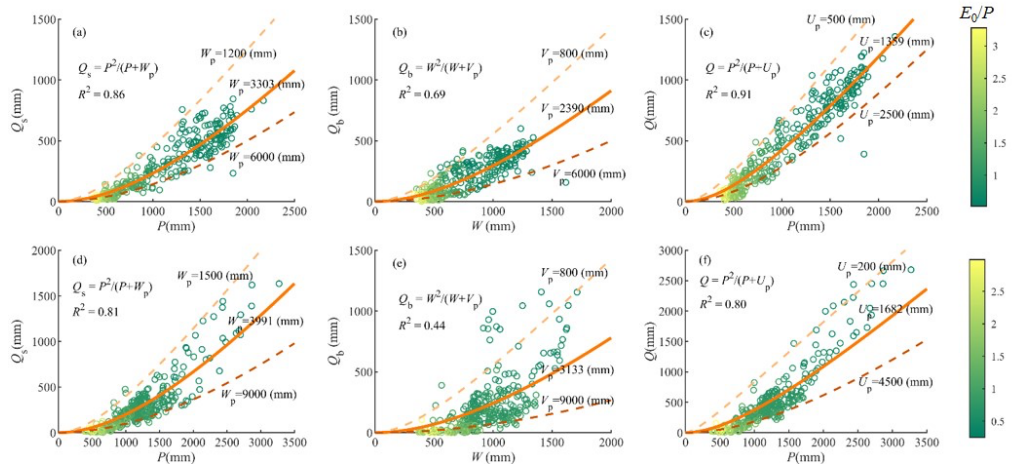
289 4.1. Inter-Catchment Variability of Runoff Components

290 We employ the MPS model to fit the relationship between mean annual available water and
291 runoff components. In China, as shown in Figure 4(a-c), the MPS model performs well in
292 describing runoff components variability between catchments, with R^2 values of 0.86, 0.68 and
293 0.91 for fitting Q_s , Q_b and Q , respectively. The solid lines are the best-fitted MPS curves derived
294 using the least squares fitting algorithm, implying the median values of different parameters. We
295 also give the potential upper and lower limits of W_p , V_p and U_p across catchments. Similarly,
296 Figure 4(d-f) illustrates that the MPS model achieves good fitting in the CONUS, with R^2 of 0.81,
297 0.44 and 0.80 for fitting Q_s , Q_b and Q , respectively. The fitted parameters in the CONUS are
298 smaller than those in China, while they have more comprehensive ranges between catchments,
299 meaning a more significant heterogeneity in climate and underlying surface.

300 Figures 4 demonstrates that the MPS model can effectively reproduce the spatial variability of
301 different runoff components along with the aridity index (E_0/P), which are primarily controlled by
302 the available water of the corresponding partition stage. The performance of MPS model to fit Q_s
303 and Q is better than that of Q_b , indicating that the factors controlling Q_b are more complicated and
304 not fully reflected in the model. With catchment properties and other factors (integrated by the
305 parameters in the MPS model) remaining unchanged, the more the available water, the higher the



306 runoff generated. Conversely, smaller parameter values are associated with greater runoff for a
 307 given amount of available water.



308 **Figure 4.** The MPS model relating (a) P versus Q_s , (b) W versus Q_b and (c) P versus Q in China
 309 and (d) P versus Q_s , (e) W versus Q_b and (f) P versus Q in the CONUS. The lines are the fitted
 310 MPS curves with best fitting (solid line) and potential upper limit and lower limit (dashed lines)
 311 parameters.

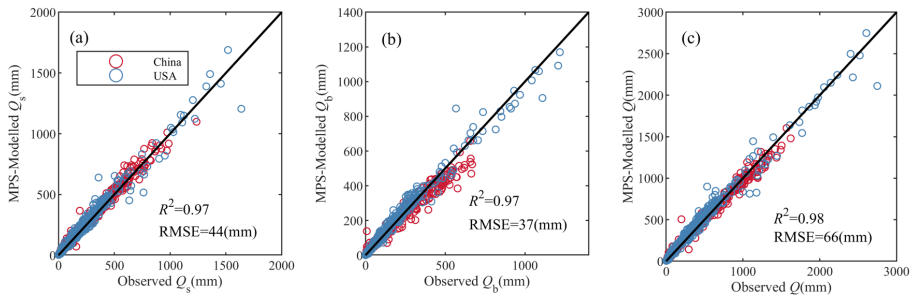
312 4.2. Validation of Runoff Components Estimation

313 Figure 5 shows the estimated mean annual Q_s , Q_b and Q in validation periods using the MPS
 314 model with inverted parameters in equation (14) in China and the CONUS. The simulated runoff
 315 components match very well with the observed, with R^2 greater than 0.97 and RMSE less than 66
 316 mm. There is no significant difference in the performance in simulating Q_s , Q_b , and Q , except for
 317 a slight underestimation in simulating Q_b of catchments in China and some in the CONUS.

318 In panels (a), (b), and (c), we observe that the scatter points for both China (red circles) and the
 319 CONUS (blue circles) are closely aligned with the 1:1 line, further underscoring the strong
 320 correlation between modeled and observed values. Specifically, the results show that the MPS
 321 model effectively captures surface flow (Q_s), baseflow (Q_b), and total runoff (Q) for both regions.
 322 Despite the generally good performance, a slight underestimation of Q_b is evident in a subset of
 323 catchments in China and, to a lesser extent, in the CONUS. However, these discrepancies are
 324 minimal and do not significantly detract from the model's overall accuracy.



326



327

Figure 5. The observed and simulated mean annual (a) surface flow, (b) baseflow and (c) total runoff by the MPS model in China (red circles) and the CONUS (blue circles).

329

Figure 6 presents the estimation of *SFC* and *BFC* in validation periods using the MPS model.

330

Similar to the simulation of Q_s , the two methods also show highly consistent estimation of *SFC*

331

(panel (a)), with R^2 of 0.94 and RMSE of 0.03. This demonstrates the MPS model's robust

332

capability to estimate the surface flow fraction in China and the CONUS, closely aligning with

333

the observed data. Panel (b) presents the estimation of *BFC*, where the MPS model achieves

334

significant accuracy, reflected by the same R^2 and RMSE values (0.94 and 0.03, respectively).

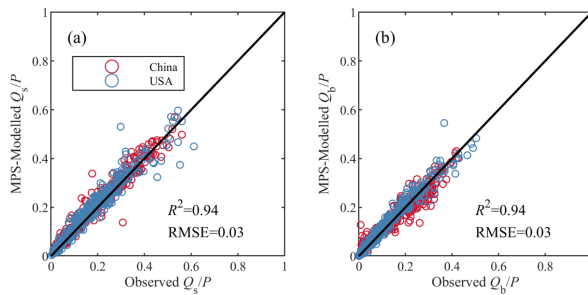
335

This strong performance indicates that the MPS model is highly effective in simulating *SFC* and

336

BFC across various catchments.

337



338

Figure 6. The observed and simulated (a) surface flow fraction (Q_s/P) and (b) baseflow fraction (Q_b/P) by the MPS model in China (red circles) and the CONUS (blue circles).

340

Figure 5 and Figure 6 document that the MPS model can effectively estimate the multi-year average of all runoff components and the proportions of precipitation allocated to runoff.

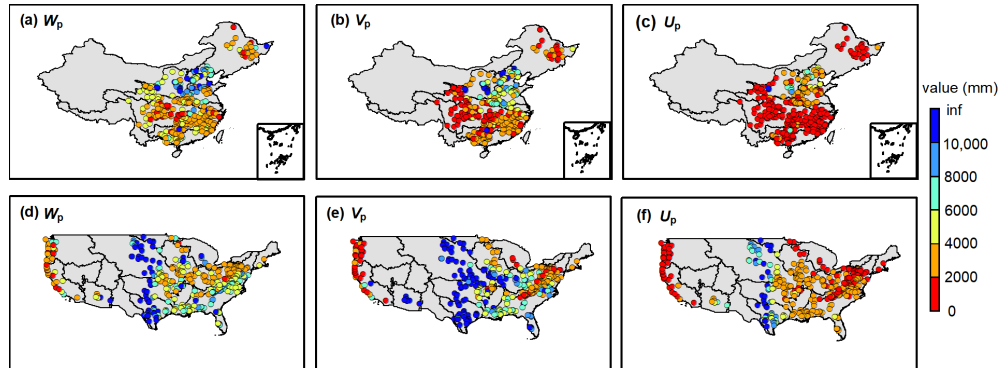
342

The good validation performance of the MPS model verified our hypothesis that the parameters in the general formulations remain stable at the mean annual time scale. The parameters reflect



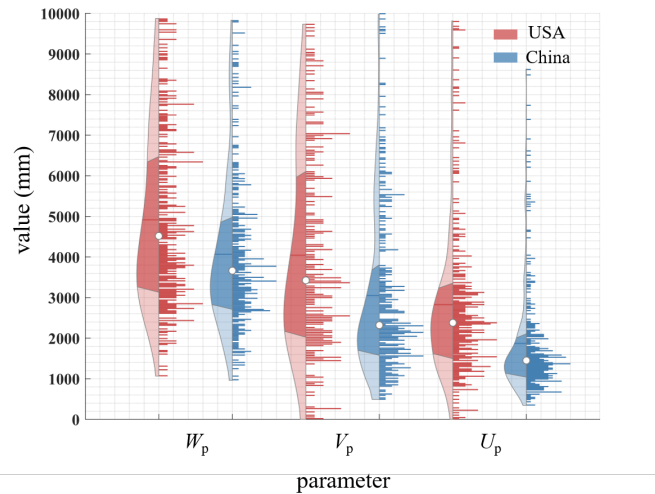
344 the comprehensive impact of climate and catchment characteristics, i.e., catchment wetting
345 potential (W_p), vaporization potential (V_p) and the upper limit of the portion remaining after
346 precipitation is allocated to runoff (U_p). As shown in Figure 7(a-c), the spatial distribution of the
347 parameters across China exhibits pronounced divergence between the northern and southern
348 catchments, as well as the eastern and the western. The W_p , V_p and U_p exhibit similar spatial
349 patterns, which can be approximately divided into two tiers from north to south. In the catchments
350 of the Songliao River Basin in the northeast, the Yangtze River Basin and Pearl River Basins in
351 the south, the parameters are relatively small, with W_p and U_p ranging from 0 to 2000 mm, and V_p
352 from 0 to 4000 mm, resulting large flow. In the catchments of the Yellow River Basin, Huaihe
353 River Basin and Haihe River Basin in the north, the parameters are quite large and usually more
354 than 5000 mm and even 8000 mm, leading to small flow. From west to east, W_p exhibits higher
355 values in the Yangtze and Yellow Rivers Basin sources, whereas V_p and U_p are smaller in the
356 source regions. This disparity may reflect variations in the two-stage partition of precipitation,
357 contributing to spatial differences in total runoff. According to Figure 7(c), we can deduce that
358 the spatial distribution of higher total runoff in south and lower in north across China, aligning
359 with previous observational studies (He et al., 2021; He et al., 2022; Yang et al., 2019).

360 Figure 7(d-f) shows an evident west-east discrepancy of the three parameters across the
361 CONUS. Typically, W_p , V_p and U_p of the catchments in the west coast and eastern regions are less
362 than 5000 mm, while parameters in the central United States are extensive with values more than
363 8000 mm. This indicates relatively low flow in the central regions. Notably, the parameters upper
364 limits in the catchments of the CONUS are significantly higher than those in China. The
365 extremely large values may be associated with significant parameter uncertainty (Gnann et al.,
366 2019). Figure 7 demonstrates that the values of the three parameters are larger in arid catchments
367 and their spatial patterns are similar to that of climate zoning, which provides insights for
368 parameterization.



369
370 **Figure 7.** The (a) wetting potential (W_p), (b) vaporization potential (V_p) and (c)
371 evapotranspiration potential (U_p) of the catchments in China and (d) wetting potential (W_p), (e)
372 vaporization potential (V_p) and (f) evapotranspiration potential (U_p) of the catchments in the
373 CONUS.

374 Figure 8 shows the violin plots of the parameters in the catchments of China and the CONUS.
375 The median values of W_p , V_p , and U_p in China are 3659 mm, 2220 mm and 1453 mm,
376 respectively. The median values of W_p , V_p , and U_p in the CONUS are 4531 mm, 3424 mm and
377 2385 mm, respectively. Overall parameters in China are smaller and denser than those in the
378 CONUS, implying a smaller variability of runoff components in China. Furthermore, the C_v value
379 of V_p (1.6 in China and 6.8 in the CONUS) is the largest, followed by U_p (0.9 in China and 1.6 in
380 the CONUS), and the smallest for W_p (0.6 in China and 1.5 in the CONUS). This indicates that
381 the parameter dispersion controlling the second partition stage of rainfall is the greatest, which
382 could partly account for the challenges in accurately estimating Q_b .

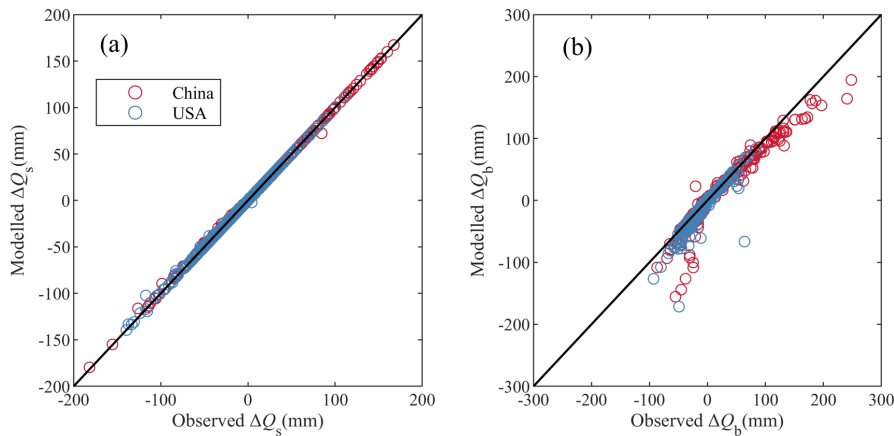


383

384 **Figure 8.** Violin plots of the parameters in the catchments of China and the CONUS. In each
385 violin plot, the left side represents the distribution, with the shaded area indicating the box plot,
386 the dot representing the mean, and the right side showing the histogram. The length of the
387 histogram represents the number of catchments (values larger than 10,000 are not shown).

388 **4.3. The Changes Attribution of Runoff Components**

389 The metrics to evaluate the attribution results between the changes of the observed and
390 simulated runoff components are shown in Table 2. We use the MPS model to estimate the
391 changes of Q_s (ΔQ_s), Q_b (ΔQ_b) and Q (ΔQ) from two long-term periods by equation (17) and
392 (20), and for comparison, we use the Budyko framework to estimate ΔQ , which is considered as
393 the changes induced by P , E_0 , and parameter n (the calculation formulations can refer Zhang et al.
394 (2018)). The estimated and observed runoff components variations exhibit high consistency
395 (Figure 9), with an R^2 of 0.99 and RMSE of 1.6 mm of ΔQ_s attribution and R^2 of 0.88 and RMSE
396 of 18 mm of ΔQ_b attribution, respectively. As for ΔQ attribution, both the MPS model and the
397 Budyko framework can attain satisfactory performance, while the MPS model has a higher R^2
398 (0.91) than the Budyko framework (0.89). Table 2 demonstrates that the MPS model can
399 accurately quantify changes in runoff components over two periods. Subsequently, we quantify
400 the contribution of precipitation and other factors (encoded by parameter W_p and V_p) to ΔQ_s and
401 ΔQ_b .



402

403 **Figure 9.** The observed and modelled (a) surface flow and (b) baseflow by the MPS model.

404

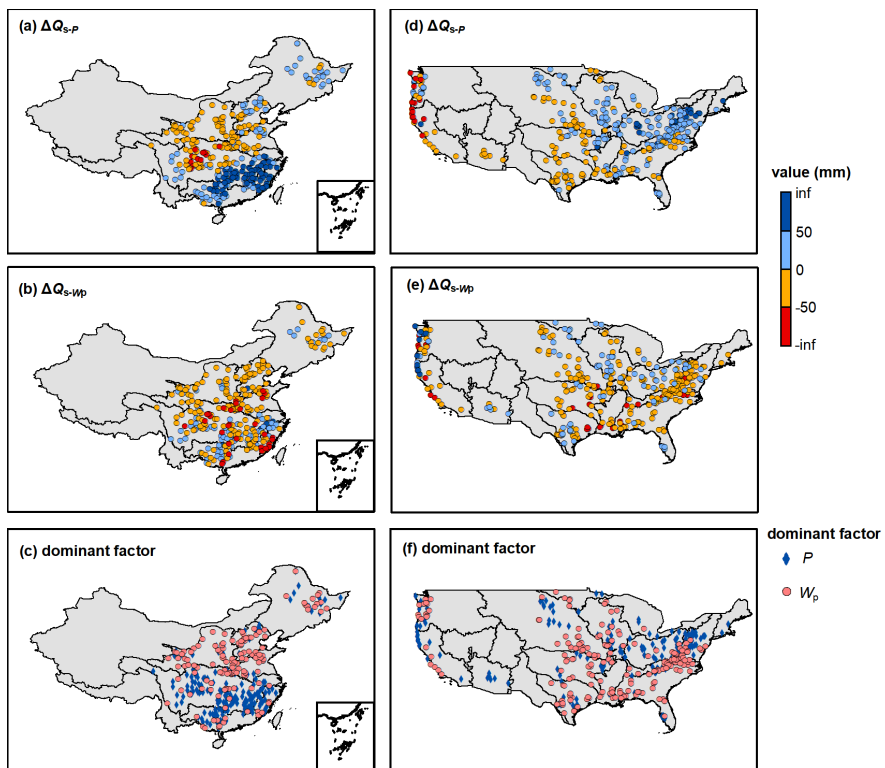
Table 2. The metrics of the attribution validation

Variables	R^2	RMSE (mm)
ΔQ_s	0.99	1.6
ΔQ_b	0.90	16
ΔQ (the MPS model)	0.91	42
ΔQ (the Budyko framework)	0.89	41

405 Figure 10 shows the ΔQ_s induced by P (ΔQ_{s-P}) and other factors (ΔQ_{s-W_p}) along with the
 406 dominant factor in the catchments of China and the CONUS. From 1960-1990 to 1991-2000 in
 407 China, the multi-year variation in P has resulted in Q_s change ranging from -105 to 344 mm,
 408 mainly increasing Q_s in the catchments of the Songliao River Basin, the middle and lower
 409 Yangtze River Basin, the Southeast River Basin and Pearl River Basin, and decreasing Q_s in the
 410 catchments of the Yellow River Basin and the upper Yangtze River Basin (Figure 10(a)). The
 411 variations of other factors, such as land use/cover change and human activities, have resulted in
 412 Q_s change ranging from -186 to 124 mm, primarily decreases Q_s in 70% catchments (Figure
 413 10(b)). P and other W_p are the dominant factor altering Q_s in southern and northern China,
 414 respectively (Figure 10(c)). From 1980-2000 to 2000-2014 in the CONUS, variation in P has
 415 resulted in Q_s change ranging from -469 to 149 mm, mainly increasing Q_s in the catchments of
 416 Interior Plains (except Great Plains), Coastal Plain, Interior highlands and Appalachian Plain, and
 417 decreasing Q_s in the catchments of the Great Plains and Pacific Mountains (the physiographic



418 divisions are referred to Wu et al. (2021)) (Figure 10(d)). The variations of other factors have
419 resulted in Q_s change ranging from -230 to 467 mm, primarily decreases Q_s in 75% catchments
420 (Figure 10(e)). The catchments in the CONUS dominated by P and W_p account for 43% and 57%,
421 respectively (Figure 10(f)).

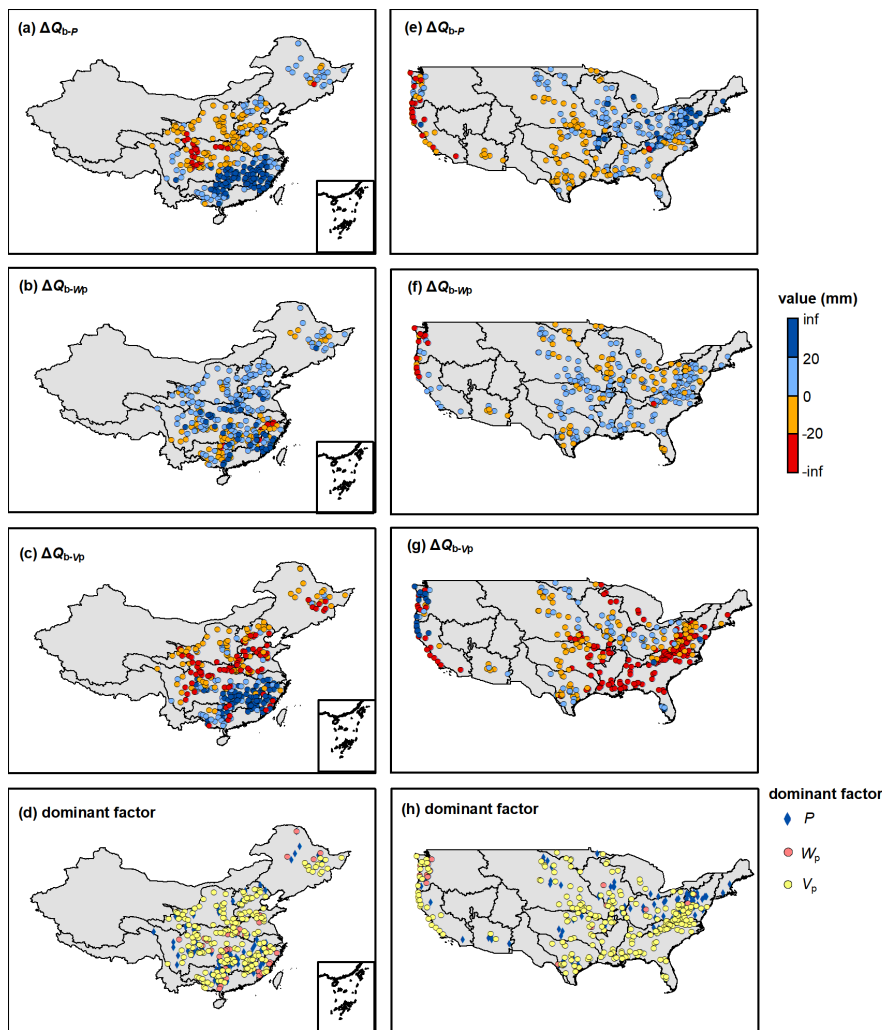


422
423 **Figure 10.** The surface flow change induced by precipitation and wetting potential (W_p) along
424 with the dominant controlling factor.

425 Figure 11 shows the ΔQ_b induced by P (ΔQ_{b-P}), W_p (ΔQ_{b-W_p}) and V_p (ΔQ_{b-V_p}) in the
426 catchments of China and the CONUS. The spatial pattern of the effect of P on Q_b is similar to that
427 of the Q_s , resulting in Q_b change from -38 to 79 mm in China (Figure 11(a)) and -129 to 92 mm in
428 the CONUS (Figure 11(e)), respectively. Catchment wetting potential has a positive effect on Q_b
429 in 70% and 75% catchments of China and the CONUS, respectively (Figure 11(b) and (f)), mainly
430 in the northern China and the Interior Highlands, Coastal Plain and Appalachian Highlands of the
431 CONUS. Vaporization potential has a negative effect on Q_b in 56% and 77% catchments of China
432 and the CONUS, respectively, mainly in the upper Yangze River Basin and northern China and



433 the central and southeastern CONUS (Figure 11(c)and (g)). Although V_p is the dominant factor
434 controlling Q_b variation in most catchments in both China (62%) and the CONUS (71%) (Figure
435 11(d)and (h)), the contributions of the P , W_p and V_p are not significantly discrepant in terms of
436 magnitude.



437
438 **Figure 11.** The baseflow change induced by precipitation, wetting potential (W_p) and
439 vaporization potential (V_p) along with the dominant controlling factor.

440 Overall, Figure 10 and 11 illustrate that the variation of Q_s is jointly controlled by P and other
441 factors, while the variation of Q_b is mainly influenced by V_p . This demonstrates that Q_s is closely
442 related to rainfall and soil storage capacity, while Q_b is more affected by catchment attributes,

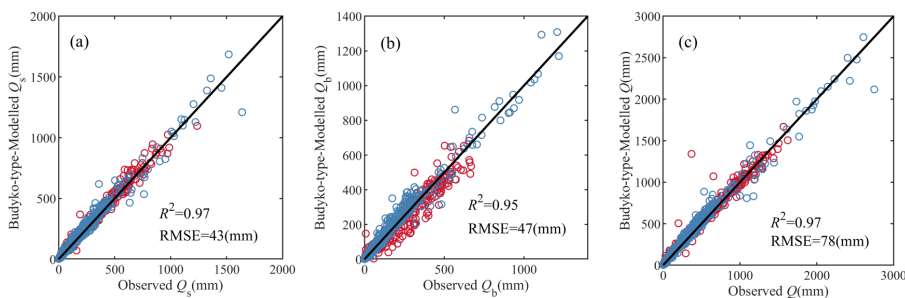


443 atmospheric water and energy demand, etc. In regions where runoff components are reduced,
444 focus should be given to the risks of drought and river discontinuity; conversely, in areas
445 experiencing runoff components increase, there is a need to guard against the risk of flooding.

446 5. Discussion

447 5.1. Superiorities of the MPS Model

448 The researches about long-term runoff components quantification and attribution are currently
449 fragmented and region-specific (Beck et al., 2013; Gnann, 2021). This study has developed a
450 general formulation (the MPS model) through observational data analysis and theoretical
451 derivation based on the Ponce-Shetty model, unveiling the patterns of variability in different
452 runoff components at mean annual time scale. Compared to the commonly used Budyko-type
453 formulations, it can not only estimate mean annual Q and Q_b , but also can depict the variability of
454 Q_s . Figure 12 shows the estimated mean annual runoff components by the Budyko-type
455 formulations (equations in the second and fifth rows of Table 1 in this paper). The Budyko-type
456 formulations also achieve good validation performance, with R^2 greater than 0.95 and RMSE less
457 than 78 mm. Although the MPS model and the Budyko-type formulations are comparable in
458 terms of R^2 , especially with almost equal simulation results of Q_s , the MPS model reduced the
459 RMSE values by 10 mm and 12 mm for estimating Q_b , respectively.



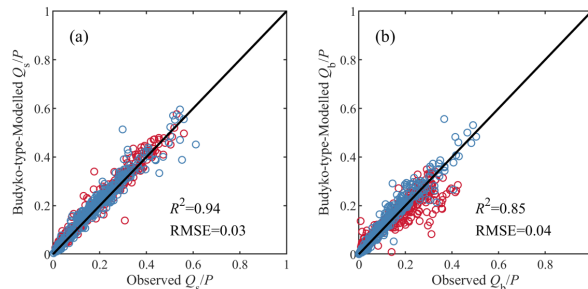
460
461 **Figure 12.** The observed and simulated mean annual (a) surface flow, (b) baseflow and (c) total
462 runoff by the Budyko-type formulations in China (red circles) and the CONUS (blue circles).

463 Figure 13 presents the estimation of SFC and BFC in validation periods using the Budyko-type
464 formulations. The two methods also show highly consistent estimation of SFC , with R^2 of 0.94



465 and RMSE of 0.03. However, the Budyko-type formulations underestimate the *BFC* of most
466 catchments in China, while the MPS model greatly improves the simulation accuracy of *BFC*.

467



468 **Figure 13.** The observed and simulated (a) surface flow fraction (Q_s/P) and (b) baseflow fraction
469 (Q_b/P) by the MPS model in China (red circles) and the CONUS (blue circles).

470 In conclusion, the MPS model has comparable capability in simulating Q_s and *SFC* to that of
471 Budyko-type formulations. Moreover, it outperforms Budyko-type formulations in estimating Q_b
472 and Q , and reveals superiority in estimating *BFC*. By characterizing runoff components as
473 functions of available water at corresponding stages with a composite parameter, the MPS model
474 is more concise in form and eliminates additional and complex parameter computations, thereby
475 facilitating broader application in large-sample investigations.

476 In addition to precisely quantifying runoff components and the allocation of precipitation, this
477 model has innovatively attributed the contributions of different factors on the changes of Q_s and
478 Q_b . Our results show that the variation of Q_s is jointly controlled by P and other factors. P plays
479 an dominant role in the variation of Q_s in the catchments of the Yangtze River Basin, Southeast
480 Basin and Pearl River Basin of China and the west coast of the CONUS, where precipitation has
481 been reported to have undergone significant changes (Li et al., 2021; Mallakpour and Villarini,
482 2017; Massoud et al., 2020; Xu et al., 2022). This is possibly due to more extreme precipitation
483 events and summer rainfall in the middle-lower Yangtze River Basin (Ye et al., 2018) and an
484 increasing trend in the frequency of heavy precipitation over large areas of the CONUS
485 (Mallakpour and Villarini, 2017). Previous studies reported that the variation of Q in these
486 regions are dominated by P (He et al., 2022; Huang et al., 2016). Now it seems that P mainly
487 affects the first allocation stage (Q_s) and consequently change total runoff. The variation of Q_b is
488 mainly influenced by V_p , indicating that we should pay more attention to the changes of



489 catchment attributes, atmospheric water and energy demand in most catchments when
490 investigating Q_b .

491 Overall, this conceptual model extracted from observed rainfall-runoff data provides a concise,
492 general and effective tool for predicting runoff components, and evaluating their responses to
493 climate and environment under global change.

494 **5.2. Parameter Interpretation**

495 In the MPS model, each runoff component is associated with a parameter that can be
496 interpreted as the upper limit of the remaining portion of available water after it has been
497 partitioned into runoff at each stage. For instance, in the first stage, precipitation is allocated to
498 surface flow and catchment wetting, with W_p representing the upper limit of catchment wetting,
499 which describes the catchment's storage capacity related to soil, topography and so on (Cheng et
500 al., 2023). For the second stage, the available water comes from catchment wetting, which is then
501 allocated to baseflow and vaporization. The parameter V_p is the upper limit of the fraction of
502 wetting returned to the atmosphere as water vapor (Ponce and Shetty, 1995). For the total runoff,
503 we consider precipitation as the available water competing with evapotranspiration, whose upper
504 limit is represented by the parameter U_p . Similar to V_p in the second stage, U_p can be regarded as
505 a sort of atmospheric water and energy limit (somewhat analogous to potential evapotranspiration)
506 and emerges from the interaction of the available energy, vegetation and other catchment
507 characteristics. To some extent, the MPS model links Q_s and Q_b with Q using P in the first
508 trade-off and V_p in the second trade-off, so that the forms of different runoff components can be
509 unified.

510 Additionally, we compared the distribution of the parameters in the MPS model with that in
511 Gnann (Gnann et al., 2019) and Siva's work (Sivapalan et al., 2011), which did not omit the
512 initial abstraction coefficients λ_s and λ_b . There is a very similar spatial pattern of W_p and V_p in
513 the CONUS. Specifically, high W_p can be seen in the middle of the United States (Great Plains)
514 and the east (southern parts of the Appalachians) (Figure 7(d)), and high V_p can be seen in the
515 middle of the United States (Great Plains) and all southern regions (Figure 7(e)). This, to some
516 extent, illustrates the rationality of the simplification of the original Ponce-Shetty model in
517 describing the spatial variability of runoff components. According to Ponce and Shetty (1995)

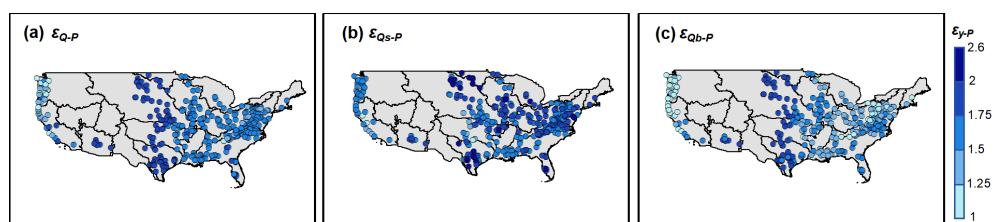


518 and Sivapalan et al. (2011), the products $\lambda_s W_p$ and $\lambda_b V_p$ are viewed as the initial abstraction to
519 generate runoff. This definition is reasonable for short-term scales, such as event and annual
520 scales. However, on the multi-annual scale, the catchment maintains a state of water balance and
521 water losses can be disregarded (Han et al., 2020). Hence, simplifying λ to zero is rational to
522 quantify and attribute runoff components and offer a new perspective on the long-term catchment
523 water balance.

524 5.3. Uncertainties and Future Improvements

525 The sensitivity of runoff to changes in climatic and environmental factors has always been
526 highly anticipated. Schaake (1990) first introduced the concept of climate elasticity coefficients to
527 quantify it, defined as the ratio of the relative change in mean annual runoff to the relative change
528 in climatic factors. Various expressions have been widely applied in evaluating the hydrological
529 response to multi-annual average climate change (Sun et al., 2014; Xu et al., 2014). The only
530 climatic factor in the MPS model is P , so we primarily focus on the elasticity of runoff
531 components to P (ε), which can be expressed as $\varepsilon_{y-P} = \frac{\partial Q_y}{\partial P} / \frac{Q_y}{P}$, quantifying the percentage of
532 runoff components change caused by 1% change in P .

533 Figure 14 shows elasticities of Q , Q_s and Q_b to P derived from the MPS model in the CONUS.
534 We compare the elasticity distribution of the work conducted by Harman et al. (2011), who did
535 not omit the initial abstraction coefficients λ . In humid catchments with the aridity index of less
536 than 1 (such as the west coast and eastern regions of the CONUS), the results from both studies
537 are very close, with elasticity values from 1 to 2. However, the MPS model noticeably
538 underestimates the runoff sensitivity to P in semi-arid and arid catchments (such as the Great
539 Plains). This may be due to the error caused by the assumption that λ is a constant when deriving
540 the MPS model.



541
542 **Figure 14.** The elasticity of (a) total runoff, (b) surface flow and (c) baseflow to precipitation



543

derived the MPS model.

544 Additionally, the secondary rainfall processes, such as initial abstraction to generate runoff,
545 precipitation intensity and seasonality should be considered in these regions, which have been
546 proven to have a significant impact in attribution analysis (He et al., 2022; Ning et al., 2022;
547 Zhang, 2015). Moreover, the potential evapotranspiration (E_0), which indicates the impact of
548 energy constraints (Huang et al., 2019; Wu et al., 2020), is quite significant in arid and semi-arid
549 catchments and should be taken into account.

550 In this paper, we interpret the parameters (i.e., W_p , V_p and U_p) as a potential upper limit of each
551 partition stage competing with corresponding runoff components following the annual
552 Ponce-Shetty model. It is intriguing to discuss whether the connotation of the parameters has
553 changed from annual to mean annual time scale. On a long-term scale, the initial abstraction
554 coefficient (i.e., λ_p and λ_W) can be simplified as zero, indicating the loss for generating runoff is
555 negligible. However, to what extent the initial abstraction coefficient affect precipitation partition
556 at shorter time scales is still under-determined. The physical and theoretical interpretation of
557 parameters and their impacts at different time scales are temporarily outside the scope of this
558 study. However, it is valuable to further research in future work.

559 The MPS model has only one parameter for controlling each runoff component, which is
560 arguably simplified but dependent on calibration, and their physical meaning needs further
561 explanation. We still need to explain the parameters in terms of regional patterns of climatic
562 and/or catchment attributes, meaning that currently this model can only be applied to gauged
563 catchments with runoff observations and challenging to transfer to ungauged basins. Cheng et al.
564 (2022) proposed two machine learning methods to characterize the parameter of the Budyko
565 framework and further employed them in estimating global runoff partition (Cheng et al., 2023).
566 Results show that parameters related to vegetation (such as root zone storage capacity, water use
567 efficiency and vegetation coverage) and climate (such as precipitation depth and climate
568 seasonality) are the primary controlling factors of the parameter. Similar work can be referred to
569 (Chen and Ruan, 2023). These investigations provide priori knowledge for quantitatively linking
570 the parameters of the MPS model to climate forcing and catchment attributes in future work.



571 6. Conclusion

572 We developed a general formulation (the MPS model) to estimate mean annual runoff
573 components as a function of available water with a synthetic parameter based on a two-stage
574 partition theory, and validated it over 662 catchments across China and the CONUS with further
575 attribution analysis. The concise MPS model provides more accurate runoff components
576 estimation and innovative attribution, offering new insights to long-term water balance and giving
577 additional superiorities toward making predictions of runoff variation under global change. The
578 main conclusions are as follows:

579 (1) The investigated catchments fit well with the MPS model, with R^2 of 0.86, 0.68 and 0.91 for
580 fitting Q_s , Q_b and Q in China and R^2 of 0.81, 0.44 and 0.80 for fitting Q_s , Q_b and Q in the CONUS,
581 implying the MPS model can well reproduce the spatial variability of different runoff
582 components.

583 (2) The MPS model effectively simulates multi-year runoff components with R^2 exceeding 0.97,
584 and the proportion of runoff components relative to precipitation with R^2 exceeding 0.94. The
585 spatial distribution of the parameters across China and the CONUS is related to that of climate
586 zoning.

587 (3) The MPS model has proved effective in quantifying the variations of runoff components
588 induced by precipitation and environmental factors. The estimated and observed ΔQ_s , ΔQ_b and
589 ΔQ exhibit high consistency, with an R^2 of 0.99 and RMSE of 1.6 mm of ΔQ_s attribution, R^2 of
590 0.90 and RMSE of 16 mm of ΔQ_b attribution and R^2 of 0.91 and RMSE of 42 mm of ΔQ
591 attribution, respectively. The variation of Q_s is jointly controlled by P and environmental factors,
592 while the variation of Q_b is mainly influenced by V_p in most catchments.

593 In general, this study proposes a general formulation for effectively estimating and attributing
594 the mean annual runoff, surface flow and baseflow. The structure is simple with few parameters
595 and clear physical significance. Its reliability has been authenticated, providing new insights for
596 analyzing watershed water resources in changing environments.

597



598 **Author Contribution**

599 Y.H. conceived and designed the study, collected and analyzed the data, and wrote the manuscript.
600 C.L participated in the study design, provided intellectual insights, and reviewed the manuscript
601 for important intellectual content. C.L. and H.Y. guided the research process and critically
602 reviewed the manuscript. All authors have read and approved the final version of the manuscript.

603 **Competing interests**

604 The authors declare that they have no conflict of interest.

605 **Acknowledgments**

606 This research was supported by the National Natural Science Foundation of China (grant no.
607 42041004 and 52309022) and the China National Key R&D Program (grant nos.
608 2021YFC3000202 and 2022YFC3002802).

609 **Data and code Availability**

610 The CAMELS data set is available at <https://ral.ucar.edu/solutions/products/camels>. The
611 hydro-meteorological data of the catchments across China can be obtained from the Zenodo
612 repository via <https://zenodo.org/records/11058118> (Li et al., 2024).

613 **Reference**

614 Addor, N., Newman, A.J., Mizukami, N. & Clark, M.P. (2017). The CAMELS data set: catchment attributes and
615 meteorology for large-sample studies. *Hydrology and Earth System Sciences*, 21(10): 5293-5313.
616 DOI:10.5194/hess-21-5293-2017

617 Al-Ghobari, H., Dewidar, A. & Alataway, A. (2020). Estimation of Surface Water Runoff for a Semi-Arid Area Using RS
618 and GIS-Based SCS-CN Method. *Water*, 12(7). DOI:10.3390/w12071924

619 Beck, H.E., van Dijk, A., Miralles, D.G., de Jeu, R.A.M., Bruijnzeel, L.A., McVicar, T.R. & Schellekens, J. (2013). Global
620 patterns in base flow index and recession based on streamflow observations from 3394 catchments. *Water
621 Resources Research*, 49(12): 7843-7863. DOI:10.1002/2013wr013918

622 Berghuijs, W.R., Larsen, J.R., van Emmerik, T.H.M. & Woods, R.A. (2017). A Global Assessment of Runoff Sensitivity
623 to Changes in Precipitation, Potential Evaporation, and Other Factors. *Water Resources Research*, 53(10):



624 8475-8486. DOI:10.1002/2017wr021593

625 Beven, K.J. & Kirkby, M.J. (1979). A physically based, variable contributing area model of basin hydrology / Un
626 modèle à base physique de zone d'appel variable de l'hydrologie du bassin versant. *Hydrological Sciences
627 Bulletin*, 24(1): 43-69. DOI:10.1080/02626667909491834

628 Budyko, M.I., (1974). Climate and life: English Edited by Miller, D. H. Academic Press, New York.

629 Chen, S. & Ruan, X.H. (2023). A hybrid Budyko-type regression framework for estimating baseflow from climate and
630 catchment attributes. *Journal of Hydrology*, 618. DOI:10.1016/j.jhydrol.2023.129118

631 Cheng, S., Hulsman, P., Koppa, A., Beck, H.E., Cheng, L. & Miralles, D.G., (2023). Global runoff partitioning based on
632 Budyko-constrained machine learning. Zenodo. DOI:<https://doi.org/10.5281/ZENODO.7932122>

633 Cheng, S.J., Cheng, L., Liu, P., Qin, S.J., Zhang, L., Xu, C.Y., Xiong, L.H., Liu, L. & Xia, J. (2021). An Analytical Baseflow
634 Coefficient Curve for Depicting the Spatial Variability of Mean Annual Catchment Baseflow. *Water
635 Resources Research*, 57(8). DOI:10.1029/2020wr029529

636 Cheng, S.J., Cheng, L., Liu, P., Zhang, L., Xu, C.Y., Xiong, L.H. & Xia, J. (2020). Evaluation of baseflow modelling
637 structure in monthly water balance models using 443 Australian catchments. *Journal of Hydrology*, 591.
638 DOI:10.1016/j.jhydrol.2020.125572

639 Cheng, S.J., Cheng, L., Qin, S.J., Zhang, L., Liu, P., Liu, L., Xu, Z.C. & Wang, Q.L. (2022). Improved Understanding of
640 How Catchment Properties Control Hydrological Partitioning Through Machine Learning. *Water Resources
641 Research*, 58(4). DOI:10.1029/2021wr031412

642 Choudhury, B.J. (1999). Evaluation of an empirical equation for annual evaporation using field observations and
643 results from a biophysical model. *Journal of hydrology (Amsterdam)*, 216(1-2): 99-110.
644 DOI:10.1016/S0022-1694(98)00293-5

645 de Graaf, I.E.M., Gleeson, T., van Beek, L.P.H., Sutanudjaja, E.H., Bierkens, M.F.P., Hylogie, Landscape functioning, G.
646 & Hylogie. (2019). Environmental flow limits to global groundwater pumping. *Nature*, 574(7776): 90-94.
647 DOI:10.1038/s41586-019-1594-4

648 Fan, Y., Li, H. & Miguez-Macho, G. (2013). Global Patterns of Groundwater Table Depth. *Science*, 339(6122): 940-943.
649 DOI:10.1126/science.1229881

650 Ficklin, D.L., Robeson, S.M. & Knouft, J.H. (2016). Impacts of recent climate change on trends in baseflow and
651 stormflow in United States watersheds. *Geophysical Research Letters*, 43(10): 5079-5088.
652 DOI:10.1002/2016gl069121

653 Gnann, S.J., (2021). Baseflow Generation at the Catchment Scale : an Investigation Using Comparative Hydrology.
654 Dissertation/Thesis Thesis.

655 Gnann, S.J., Woods, R.A. & Howden, N.J.K. (2019). Is There a Baseflow Budyko Curve? *Water Resources Research*,
656 55(4): 2838-2855. DOI:10.1029/2018wr024464

657 Hale, C.A., Carling, G.T., Nelson, S.T., Fernandez, D.P., Brooks, P.D., Rey, K.A., Tingey, D.G., Packer, B.N. & Aanderud, Z.T.
658 (2022). Strontium isotope dynamics reveal streamflow contributions from shallow flow paths during
659 snowmelt in a montane watershed, Provo River, Utah, USA. *Hydrological Processes*, 36(1).
660 DOI:10.1002/hyp.14458

661 Hall, F.R. (1968). BASE-FLOW RECESSIONS-A REVIEW. *Water Resources Research*, 4(5): 973-&.
662 DOI:10.1029/WR004i005p00973

663 Han, J.T., Yang, Y.T., Roderick, M.L., McVicar, T.R., Yang, D.W., Zhang, S.L. & Beck, H.E. (2020). Assessing the
664 Steady-State Assumption in Water Balance Calculation Across Global Catchments. *Water Resources
665 Research*, 56(7). DOI:10.1029/2020wr027392

666 Han, P.F., Sankarasubramanian, A., Wang, X.S., Wan, L. & Yao, L.L. (2023). One-Parameter Analytical Derivation in
667 Modified Budyko Framework for Unsteady-State Streamflow Elasticity in Humid Catchments. *Water*



712 Mallakpour, I. & Villarini, G. (2017). Analysis of changes in the magnitude, frequency, and seasonality of heavy
713 precipitation over the contiguous USA. *Theoretical and Applied Climatology*, 130(1-2): 345-363.
714 DOI:10.1007/s00704-016-1881-z

715 Massoud, E.C., Lee, H., Gibson, P.B., Loikith, P. & Waliser, D.E. (2020). Bayesian Model Averaging of Climate Model
716 Projections Constrained by Precipitation Observations over the Contiguous United States. *Journal of*
717 *hydrometeorology*, 21(10): 2401-2418. DOI:10.1175/JHM-D-19-0258.1

718 Milly, P.C.D. & Dunne, K.A. (2002). Macroscale water fluxes 2. Water and energy supply control of their interannual
719 variability. *Water Resour. Res.*, 38(10): 24-1-24-9. DOI:10.1029/2001WR000760

720 Morgan, R.P.C., Nearing, M. A. (Eds.). (2011). Handbook of erosion modeling. West Sussex: Wiley - Blackwell.

721 Neto, A.A.M., Roy, T., de Oliveira, P.T.S. & Troch, P.A. (2020). An Aridity Index-Based Formulation of Streamflow
722 Components. *Water Resources Research*, 56(9). DOI:10.1029/2020wr027123

723 Newman, A.J., Clark, M.P., Sampson, K., Wood, A., Hay, L.E., Bock, A., Viger, R.J., Blodgett, D., Brekke, L., Arnold, J.R.,
724 Hopson, T. & Duan, Q. (2015). Development of a large-sample watershed-scale hydrometeorological data
725 set for the contiguous USA: data set characteristics and assessment of regional variability in hydrologic
726 model performance. *Hydrology and Earth System Sciences*, 19(1): 209-223. DOI:10.5194/hess-19-209-2015

727 Ning, T., Feng, Q. & Qin, Y. (2022). Recent variations in the seasonality difference between precipitation and
728 potential evapotranspiration in China. *International journal of climatology*, 42(7): 3616-3632.
729 DOI:10.1002/joc.7435

730 Penman, H.L. (1948). Natural evaporation from open water, bare soil and grass. *Proc. R. Soc. London Ser. Math. Phys.*
731 *Sci.* 193 (1032), 120. DOI: <https://doi.org/10.1098/rspa.1948.0037>

732 Ponce, V.M. & Shetty, A.V. (1995). A CONCEPTUAL-MODEL OF CATCHMENT WATER-BALANCE .1. FORMULATION AND
733 CALIBRATION. *Journal of Hydrology*, 173(1-4): 27-40. DOI:10.1016/0022-1694(95)02739-c

734 Price, K., Jackson, C.R., Parker, A.J., Reitan, T., Dowd, J. & Cyterski, M. (2011). Effects of watershed land use and
735 geomorphology on stream low flows during severe drought conditions in the southern Blue Ridge
736 Mountains, Georgia and North Carolina, United States. *Water Resources Research*, 47.
737 DOI:10.1029/2010wr009340

738 Roderick, M.L. & Farquhar, G.D. (2011). A simple framework for relating variations in runoff to variations in climatic
739 conditions and catchment properties. *Water Resour. Res.*, 47(12): n/a. DOI:10.1029/2010WR009826

740 Schaake, J.C., (1990). From climate to flow, in: climate change and U.S. water resources, edited by: Waggoner, P. E.,
741 chap. 8. John Wiley, New York.

742 SCS, (1972). National Engineering Handbook, section 4. Soil Conservation Service USDA, Washington, DC.

743 Shen, Y. & Xiong, A.Y. (2016). Validation and comparison of a new gauge-based precipitation analysis over mainland
744 China. *International Journal of Climatology*, 36(1): 252-265. DOI:10.1002/joc.4341

745 Shi, W., Huang, M., Gongadze, K. & Wu, L. (2017). A Modified SCS-CN Method Incorporating Storm Duration and
746 Antecedent Soil Moisture Estimation for Runoff Prediction. *Water Resources Management*, 31(5):
747 1713-1727. DOI:<https://doi.org/10.1007/s11269-017-1610-0>

748 Singh, S.K., Pahlow, M., Booker, D.J., Shankar, U. & Chamorro, A. (2019). Towards baseflow index characterisation at
749 national scale in New Zealand. *Journal of Hydrology*, 568: 646-657. DOI:10.1016/j.jhydrol.2018.11.025

750 Sivapalan, M., Yaeger, M.A., Harman, C.J., Xu, X.Y. & Troch, P.A. (2011). Functional model of water balance variability
751 at the catchment scale: 1. Evidence of hydrologic similarity and space-time symmetry. *Water Resources*
752 *Research*, 47. DOI:10.1029/2010wr009568

753 Sun, Y., Tian, F.Q., Yang, L. & Hu, H.P. (2014). Exploring the spatial variability of contributions from climate variation
754 and change in catchment properties to streamflow decrease in a mesoscale basin by three different
755 methods. *Journal of Hydrology*, 508: 170-180. DOI:10.1016/j.jhydrol.2013.11.004



756 Troch, P.A., Martinez, G.F., Pauwels, V.R.N., Durcik, M., Sivapalan, M., Harman, C., Brooks, P.D., Gupta, H. & Huxman,
757 T. (2009). Climate and vegetation water use efficiency at catchment scales. *Hydrological Processes*, 23(16):
758 2409-2414. DOI:10.1002/hyp.7358

759 Wallace, S., Biggs, T., Lai, C.-T. & McMillan, H. (2021). Tracing sources of stormflow and groundwater recharge in an
760 urban, semi-arid watershed using stable isotopes. *Journal of Hydrology: Regional Studies*, 34: 100806.
761 DOI:<https://doi.org/10.1016/j.ejrh.2021.100806>

762 Wang, D. & Wu, L. (2013). Similarity of climate control on base flow and perennial stream density in the Budyko
763 framework. *Hydrology and earth system sciences*, 17(1): 315-324. DOI:10.5194/hess-17-315-2013

764 Wang, H., Liu, J., Klaar, M., Chen, A., Gudmundsson, L. & Holden, J. (2024). Anthropogenic climate change has
765 influenced global river flow seasonality. *Science (New York, N.Y.)*, 383(6686): 1009-1014.
766 DOI:10.1126/science.adl9501

767 Wu, J.W., Miao, C.Y., Duan, Q.Y., Lei, X.H., Li, X.Y. & Li, H. (2019). Dynamics and Attributions of Baseflow in the
768 Semiarid Loess Plateau. *Journal of Geophysical Research-Atmospheres*, 124(7): 3684-3701.
769 DOI:10.1029/2018jd029775

770 Wu, S., Zhao, J., Wang, H. & Sivapalan, M. (2021). Regional Patterns and Physical Controls of Streamflow Generation
771 Across the Conterminous United States. *Water resources research*, 57(6): n/a. DOI:10.1029/2020WR028086

772 Wu, Y.Y., Fang, H.W., Huang, L. & Ouyang, W. (2020). Changing runoff due to temperature and precipitation
773 variations in the dammed Jinsha River. *Journal of Hydrology*, 582. DOI:10.1016/j.jhydrol.2019.124500

774 Xu, F., Zhou, Y.Y. & Zhao, L.L. (2022). Spatial and temporal variability in extreme precipitation in the Pearl River Basin,
775 China from 1960 to 2018. *International Journal of Climatology*, 42(2): 797-816. DOI:10.1002/joc.7273

776 Xu, X.Y., Yang, D.W., Yang, H.B. & Lei, H.M. (2014). Attribution analysis based on the Budyko hypothesis for detecting
777 the dominant cause of runoff decline in Haihe basin. *Journal of Hydrology*, 510: 530-540.
778 DOI:10.1016/j.jhydrol.2013.12.052

779 Yang, H.B., Qi, J., Xu, X.Y., Yang, D.W. & Lv, H.F. (2014). The regional variation in climate elasticity and climate
780 contribution to runoff across China. *Journal of Hydrology*, 517: 607-616. DOI:10.1016/j.jhydrol.2014.05.062

781 Yang, H.B., Yang, D.W., Lei, Z.D. & Sun, F.B. (2008). New analytical derivation of the mean annual water-energy
782 balance equation. *Water Resources Research*, 44(3). DOI:10.1029/2007wr006135

783 Yang, W.T., Long, D. & Bai, P. (2019). Impacts of future land cover and climate changes on runoff in the mostly
784 afforested river basin in North China. *Journal of Hydrology*, 570: 201-219.
785 DOI:10.1016/j.jhydrol.2018.12.055

786 Yao, L.L., Sankarasubramanian, A. & Wang, D.B. (2021). Climatic and Landscape Controls on Long-Term Baseflow.
787 *Water Resources Research*, 57(6). DOI:10.1029/2020wr029284

788 Ye, X., Xu, C., Zhang, D. & Li, X. (2018). Variation of Summer Precipitation and Its Connection with Asian Monsoon
789 System in the Middle-lower Yangtze River Basin. *Scientia Geographica Sinica*, 38(7): 1174-1182.

790 Yin, J.B., Gentile, P., Zhou, S., Sullivan, S.C., Wang, R., Zhang, Y. & Guo, S.L. (2018). Large increase in global storm
791 runoff extremes driven by climate and anthropogenic changes. *Nature Communications*, 9.
792 DOI:10.1038/s41467-018-06765-2

793 Zhang, D. (2015). On the effects of seasonality of precipitation and potential evapotranspiration on catchment
794 hydrologic partitioning., Tsinghua University, Beijing, China, p. 150. pp.

795 Zhang, J.L., Zhang, Y.Q., Song, J.X. & Cheng, L. (2017). Evaluating relative merits of four baseflow separation methods
796 in Eastern Australia. *Journal of Hydrology*, 549: 252-263. DOI:10.1016/j.jhydrol.2017.04.004

797 Zheng Mingguo, S.L. (2014). Recent change of runoff and its components of baseflow and surface runoff in response
798 to climate change and human activities for the Lishui watershed of southern China (in Chinese).
799 *Geographical Research*, 33(02): 237-250.